buildings

MDPI

Article

Experimental Investigation and Numerical Analyses on Cyclic Behavior of the Prefabricated Concrete Frame Infilled with CFS-CLPM Composite Walls

Peifang Hu [1], Yong Liu [1,2,*], Jingfeng Wang [1,2], Wanqian Wang [1,2] and Guangdong Pan [1]

[1] School of Civil Engineering, Hefei University of Technology, Hefei 230009, China
[2] Anhui Key Laboratory of Civil Engineering Structures and Materials, Hefei 230009, China
* Correspondence: yongliu@hfut.edu.cn; Tel.: +86-5516-2901-434

Abstract: A novel CFS composite wall filled with cement-based lightweight polymer material (CFS-CLPM composite wall) has been proposed and proven to have excellent architectural and mechanical performance. To promote its application in prefabricated concrete (PC) frame structures, two full-scale specimens were designed and tested under cyclic loading to investigate the failure mode, hysteretic response and energy dissipation of the PC frame infilled with the CFS-CLPM composite wall. The experimental results indicated that CFS-CLPM composite walls can significantly improve the lateral behavior of the PC frame in terms of load capacity, elastic stiffness and energy dissipation capacity, while slightly reducing its ductility because of the infill-frame interaction. Subsequently, finite element (FE) analyses for the PC frame infilled with CFS-CLPM composite walls were developed and verified against the experimental results. The force-transferring mechanisms between the PC frame and the CFS-CLPM composite walls were revealed by analyzing the stress distributions. The parametric analyses demonstrated that the influential parameters for lateral resistances of the PC frame structure infilled with CFS-CLPM composite walls were the strength of CLPM, the span-to-height ratio and the thickness of CFS-CLPM composite walls. Finally, a formula considering the mechanical contribution of the CFS-CLPM composite wall was proposed to predict the elastic lateral stiffness of the structures. The results of this study could provide a basis for the application of CFS-CLPM composite walls in PC frame structures.

Keywords: CFS-CLPM composite walls; PC frames; cyclic behavior; numerical analyses; elastic stiffness

Citation: Hu, P.; Liu, Y.; Wang, J.; Wang, W.; Pan, G. Experimental Investigation and Numerical Analyses on Cyclic Behavior of the Prefabricated Concrete Frame Infilled with CFS-CLPM Composite Walls. *Buildings* **2022**, *12*, 1991. https://doi.org/10.3390/buildings12111991

Academic Editor: Abdelhafid Khelidj

Received: 24 October 2022
Accepted: 12 November 2022
Published: 16 November 2022

1. Introduction

Cold-formed steel (CFS) walls filled with lightweight materials are novel composite walls developed from CFS structures, and have advantages of uniform quality, low weight, easy installation and convenient transportation [1–6]. Moreover, the lightweight fillers are usually made of industrial waste [7–9], which just meets the demand of green buildings and low-carbon society. Thus, the development and investigation of CFS composite walls filled with lightweight materials have been a hot topic. Many studies [4,10–12] investigating the structural performance of CFS composite walls filled with different lightweight materials indicated that the lightweight fillers could not only restrain the local buckling of the CFS frame effectively, but also improve the axial compressive capacity, cyclic performance and ductility.

Among these novel composite walls, CFS composite walls filled with cement-based lightweight polymer material (CFS-CLPM composite walls in abbreviation) was proposed by Wang et al. [12] as shown in Figure 1. The investigations of the CFS-CLPM composite walls have confirmed that such novel composite walls exhibited excellent axial compressive and cyclic performance [12,13]. Accordingly, industrial production lines have been

established to prefabricate the CFS-CLPM composite walls, and they have been widely used as bearing walls or shear walls in low- and multi-rise buildings in China (Figure 2).

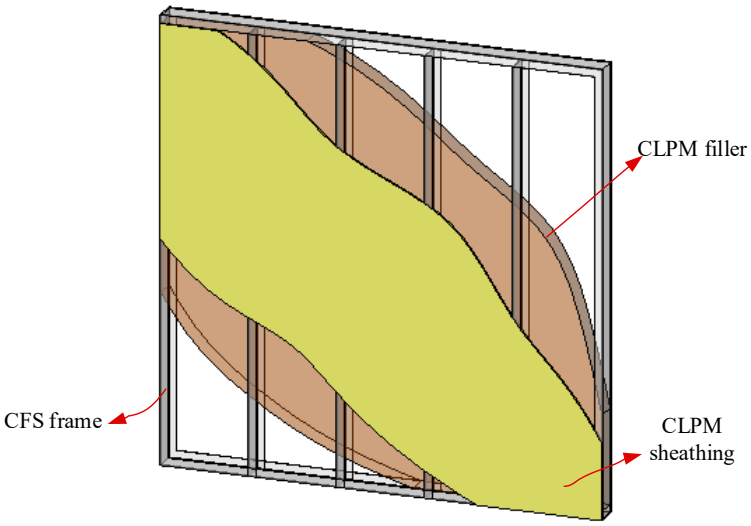

Figure 1. Configurations of CFS-CLPM composite walls.

Figure 2. Buildings with CFS-CLPM composite walls.

Furthermore, owing to the contribution of lightweight polymer material, CFS-CLPM composite walls are 800 kg/m^3 in density, which is much lighter than concrete, and have superior performance in sound insulation, thermal insulation and fire resistance than conventional CFS composite walls [13]. The CFS frame in the CFS-CLPM composite walls also made it easier to install using steel connectors. Combined with the excellent mechanical performance, CFS-CLPM composite wall is also a good option for walls in prefabricated frame structures. Prefabricated building is one of the important initiatives to achieve building industrialization and green construction, which have been vigorously promoted by the government in China. Owing to the popularity of concrete structures, prefabricated concrete (PC) buildings have gained great attention and are widely used in residential buildings and office buildings. Therefore, it is of great significance to apply CFS-CLPM composite walls into PC frame structures.

Recently, CFS walls have been introduced into frame structures by scholars to promote favorable CFS walls in high-rise buildings. Nevertheless, research on frame structure with CFS walls is still in its infancy so far. Wang et al. [14] conducted cyclic tests on the steel frame infilled with CFS composite walls. The experimental results showed that the steel frame cooperated well with the CFS composite walls and the lateral load capacity of this structure was determined by superposing shear strengths of the steel frame and the CFS composite walls. Wang et al. [15] reported that the sheathed CFS walls improved the progressive collapse capacity of steel frames but decreased the ductility. Kildashti et al. [16] proposed a

hot-rolled steel knee-braced frames with CFS stud walls system. The nonlinear analyses indicated that CFS contribution to lateral loads can improve the seismic performance of the proposed system. However, studies on PC frames cooperating with CFS walls, especially CFS-CLPM composite walls, have not been reported.

To promote the application of CFS-CLPM composite walls in PC frame structures, it is significant to study the performance of the PC frames with CFS-CLPM composite walls. In this paper, two full-scale specimens were tested under cyclic loading to investigate the performance of PC frame infilled with CFS-CLPM composite walls. The effect of CFS-CLPM composite walls on the failure mode, hysteretic response, energy dissipation and horizontal displacement-strain response of the PC frame were studied. In addition, the numerical simulation using ABAQUS software was performed to explore the working mechanism of the PC frame infilled with CFS-CLPM composite walls under horizontal loads. Finally, a superposition formula with a good degree of accuracy was proposed to predict the elastic lateral stiffness of the structures. The results of this study could provide a basis for the application of CFS-CLPM composite walls in PC frame structures.

2. Experimental Program

2.1. Test Specimens

Two specimens, including one bare prefabricated concrete frame (PCF) and one prefabricated concrete frame infilled with CFS-CLPM composite walls (PCFW), were designed and examined under cyclic loads. The PC frames of two specimens were designed with identical configurations. Figure 3a illustrated the dimensional details of the PC frame, which is 3340 mm in span and 3030 mm in height. The PC frame contained precast columns with a dimension of 300 mm × 300 mm ($b \times h$), precast beams with a dimension of 200 mm × 350 mm ($b \times h$), and foundations with a dimension of 500 mm × 570 mm ($b \times h$), as shown in Figure 3b. These PC members adopted concrete with a nominal compressive strength of 40 Mpa and hot-rolled ribbed bars with a yield strength of 400 Mpa. In the assembly process of the PC frames (Figure 4), firstly, the precast foundation, columns and beams were installed to produce a frame. Next, the precast columns were fixed on the foundation by filling sleeves with high-strength concrete grouts [17]. The depth of reinforcements of columns inserted into sleeves with a length of 340 mm was 150 mm. Finally, the concrete with a nominal compressive strength of 50 Mpa was poured into beam-column joints [18,19].

For the specimen PCFW, the wall was assembled with prefabricated separated CFS-CLPM composite walls. In accordance with Ref. [13], configurations of separated CFS-CLPM composite walls and splicing connections of the walls were determined. Single galvanized C-section steel (89 mm × 41 mm × 11 mm × 0.9 mm) with a nominal strength of 550 Mpa was selected as studs and tracks in the CFS composite walls, as illustrated in Figure 5c. The tracks were connected to studs using ST4.8-grade self-drilling screws (d = 4.8 mm) to form the CFS frame. Then cement-based lightweight polymer materials (CLPM) were poured into the space of the CFS frame. Simultaneously, sheathing layers were also poured with CLPM. The mixed proportion of CLPM is presented in Table 1. Figure 5a illustrates the configuration and frame-wall joints of the specimen PCFW. Three separated CFS-CLPM composite walls were spliced together using steel strips and ST4.8-grade self-drilling screws (d = 4.8 mm), as depicted in Figure 5b. Steel angles were used as connectors by welding to both built-in fittings and 8.8-grade hook bolts (d = 10 mm). The fittings were embedded in the PC beams and the foundations while the hook bolts were embedded in the CFS composite walls.

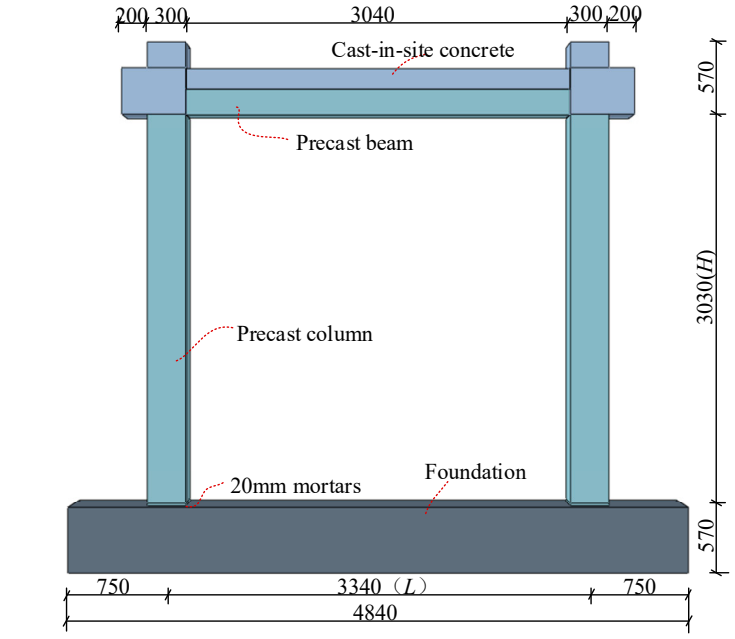

(**a**)

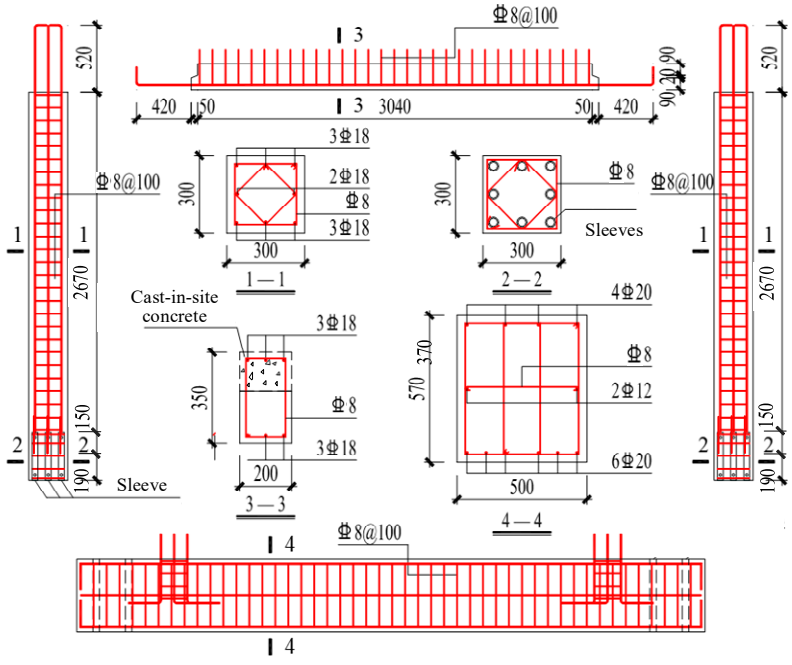

(**b**)

Figure 3. Details of PC frame: (**a**) Configurations of PC frame; (**b**) Reinforcements of precast concrete members.

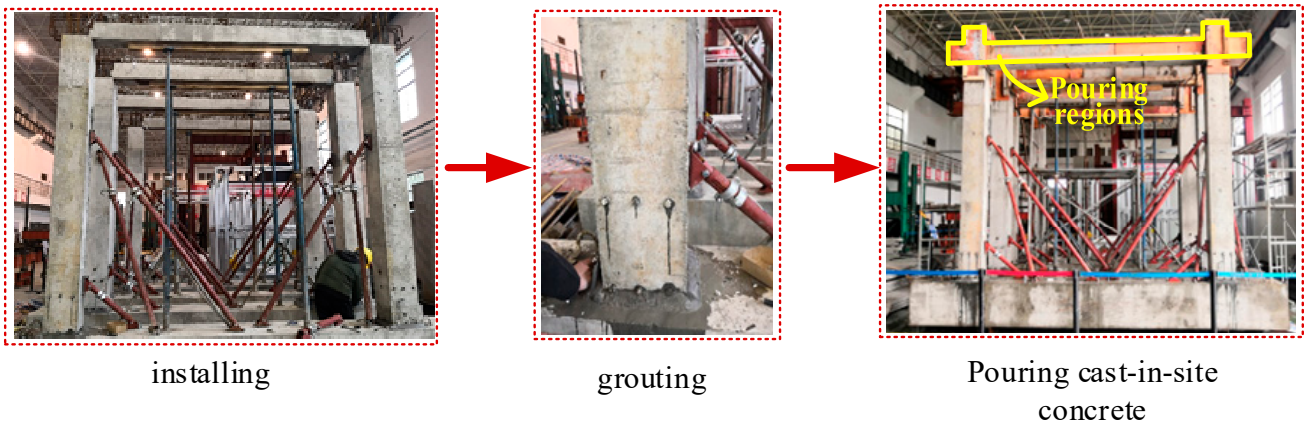

Figure 4. Assembly procedure of PC frame.

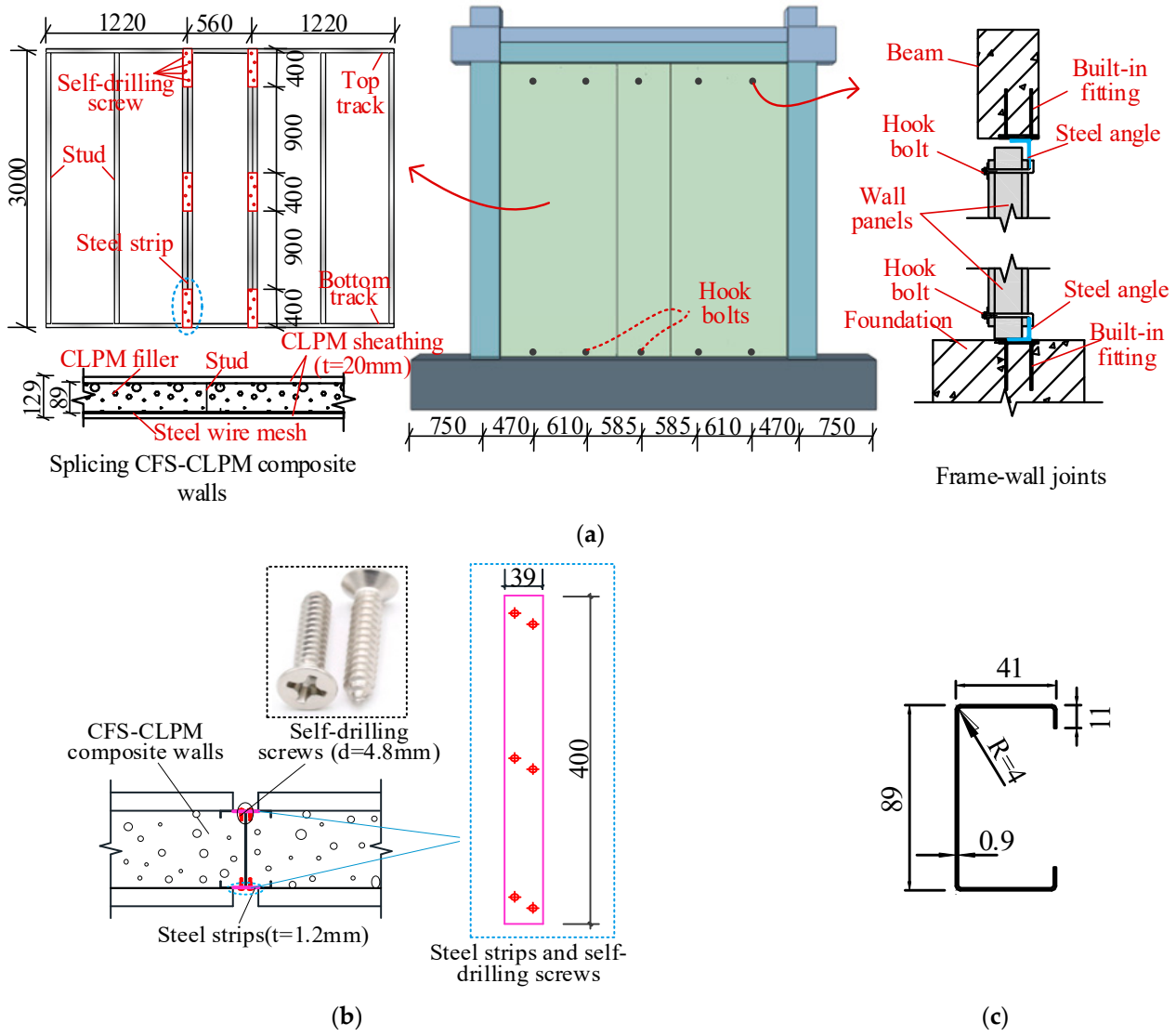

Figure 5. Details of specimen PCFW: (**a**) Configurations of specimen PCFW; (**b**) Splicing connection; (**c**) Size of C-section steel.

Table 1. Mix proportion of CLPM.

Cement (kg/m^3)	Fly Ash (kg/m^3)	Expansive Agent (kg/m^3)	Water-Reducing Agent (kg/m^3)	EPS (kg/m^3)	Water (kg/m^3)
300	65	125	2	0.6	225

2.2. Material Properties

In accordance with the Chinese Standard [20], the material properties of concrete are determined by cube coupons with the dimension of 150 mm. The measured compressive strengths of precast and cast-in-site concrete were respectively 45.2 MPa and 56.8 MPa, and the elastic modulus were 33,676.8 MPa and 35,575.6 MPa, respectively. The measured compressive strength and elastic modulus of the high-strength concrete grouts were 86.7 MPa and 34,000 MPa, respectively.

As per the Specification [21], the compressive strength and elastic modulus of CLPM were tested as 0.92 MPa and 250 MPa, respectively. The tensile coupons of the reinforcement and C-section steel were tested following the relevant provisions [22]. The mechanical characterizations of the reinforcement and C-section steel are summarized in Table 2.

Table 2. Mechanical properties of steel.

Steel Item	Thickness/ Diameter (mm)	Yield Strength (MPa)	Ultimate Strength (MPa)	Yield Strain	Elastic Modulus (MPa)
reinforcement	18	491	663	2338×10^{-6}	2.1×10^5
reinforcement	8	476	768	2268×10^{-6}	2.1×10^5
C-section steel	0.9	696	1006	3314×10^{-6}	2.05×10^5
C-section steel	1.2	695	1017	3310×10^{-6}	2.06×10^5

2.3. Test Setup and Measurements

The test setup is shown in Figure 6. The foundation was fixed on the rigid ground by four anchor bolts. Four 36 mm-diameter steel bars were used to connect the thick steel plates attached to the beam ends. The steel tube constraint device was employed to reduce hazards caused by out-of-plane collapse of specimens. The MTS hydraulic machine supplied the horizontal loads. Two vertical hydraulic jacks acting on the reaction steel frame were applied to exert axial loads at the top of each column. Two Polytetrafluoroethylene plates with high lubrication were installed between the reaction frame and the vertical hydraulic jacks to ensure that the jacks adapted to the specimens' lateral movements. In this study, twelve strain gauges numbered S1–S12 were arranged to record the longitudinal strains of reinforcements at the column ends as well as beam ends, as shown in Figure 7.

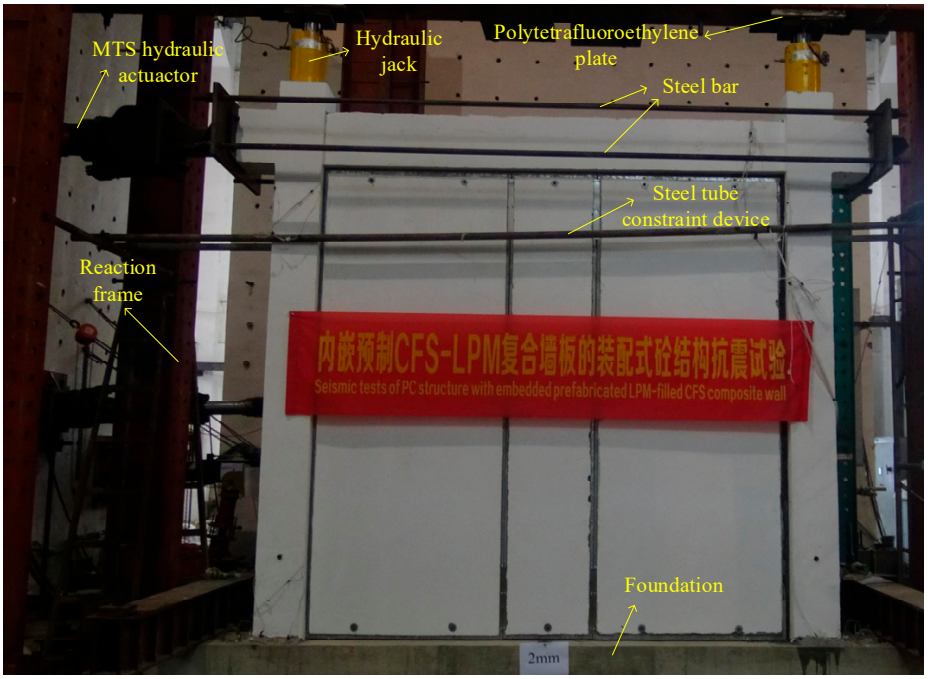

Figure 6. Test set up.

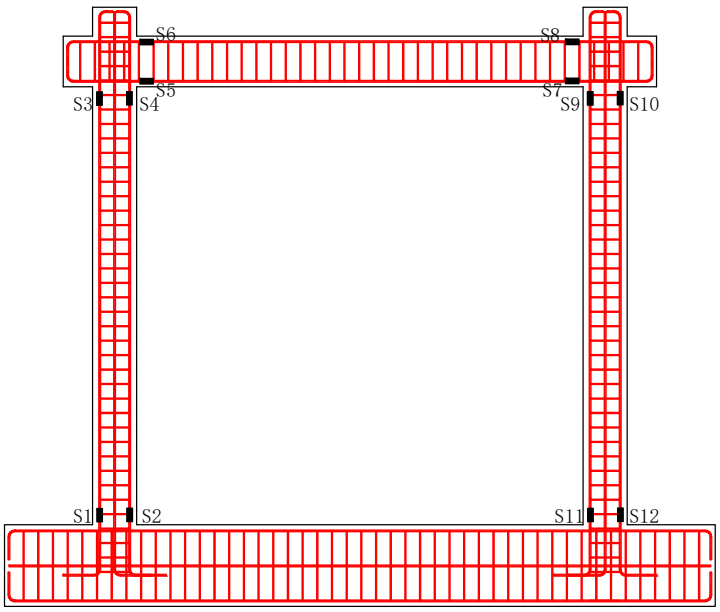

Figure 7. Strain gauges arrangement on the PC frame.

2.4. Loading Protocol

The axial load of 500 kN (calculated by an axial compression ratio of 0.3) at each top of the column remained constant during loading process. The horizontal loading was displacement-controlled as displayed in Figure 8. In the beginning, horizontal displacements of 2 mm, 3 mm, 4 mm, 5 mm, 6 mm and 7 mm were performed in one cycle per level. Afterwards, horizontal displacements of 8 mm, 16 mm, 24 mm, 32 mm, 40 mm, etc. (corresponding to the inter-story drift of 0.25%, 0.50%, 0.75%, 1.00%, 1.25% etc., respectively) were cycled three times per level. The loading procedure was terminated when the lateral load was down to 85% of the maximum lateral load or severe damage occurred on specimens.

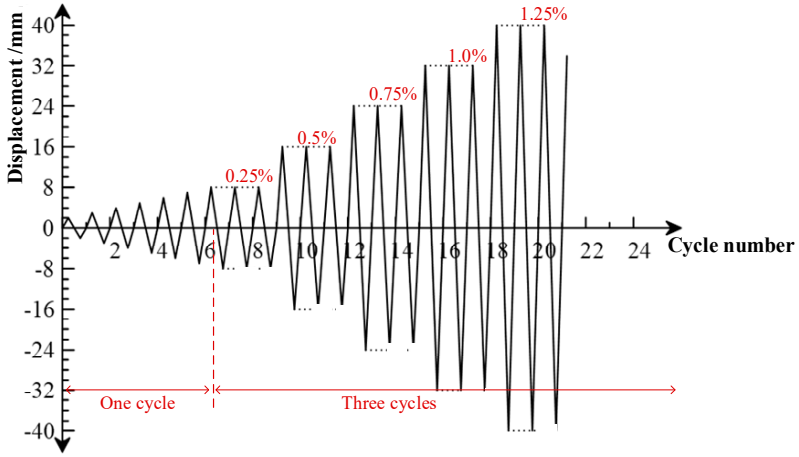

Figure 8. Loading history.

3. Experimental Results and Discussions

3.1. Failure Modes

3.1.1. Specimen PCF

Figure 9 exhibits the typical failure characteristics of specimen PCF. During the loading process with horizontal displacement of 2–7 mm, there were no damage phenomena on the specimen, indicating that the specimen was in elastic stage. When the inter-story drift increased to 0.25%, slight vertical cracks were first detected at beam ends. At the drift ratio of 0.50%, horizontal cracks occurred at the column ends near the top height of the sleeves. It showed that the strength and stiffness of columns around the length of sleeves were higher with the help of the additional steel sleeves than the rest part of the column without sleeves. Oblique cracks appeared on the beam-column joints at the drift ratio of 1.25%. As the horizontal drift increased, vertical cracks of the beam and horizontal cracks of the columns gradually widened and deepened, and eventually penetrated. When the inter-story drift was up to 4.0%, severe concrete crushing occurred at the bottom of the columns.

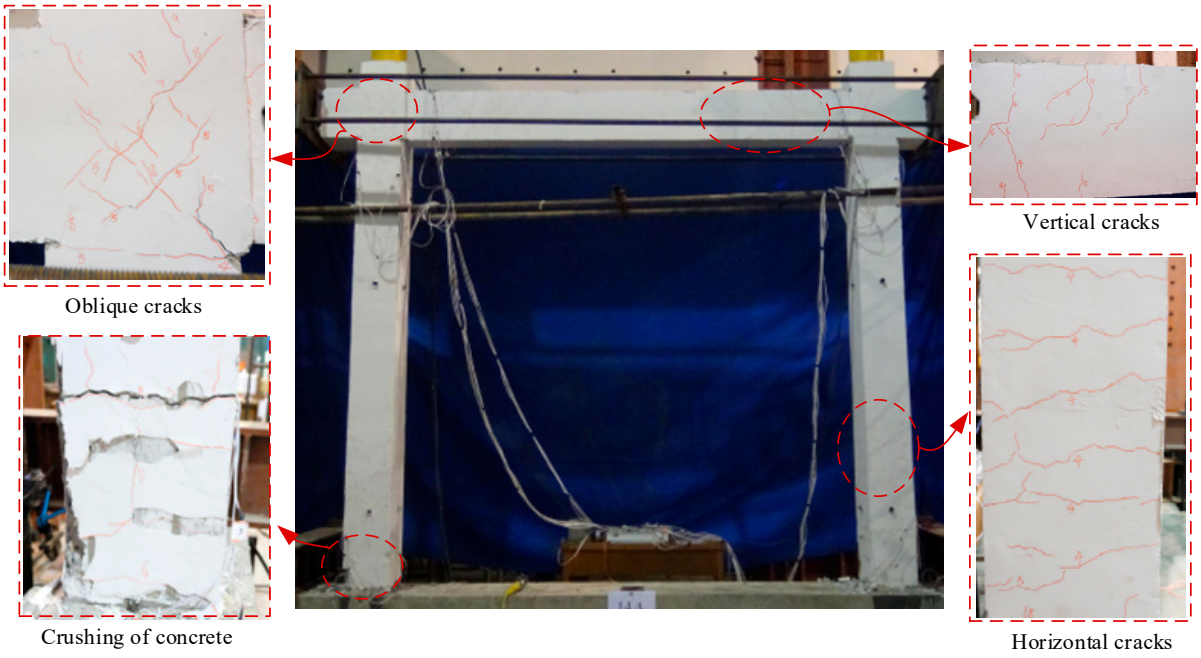

Figure 9. Failure modes of specimen PCF.

3.1.2. Specimen PCFW

In terms of the failure mode of the PC frame, specimen PCFW had similar phenomena to the specimen PCF during the cyclic loading. Concerning the failures of the CFS-CLPM composite walls, the diagonal cracks occurred and developed when the inter-story drift increased to 1.0%, as shown in Figure 10. It indicated that part of the horizontal loads was transferred to the CFS-CLPM composite walls. Moreover, the self-drilling screws on the steel strips tilted and loosened at the drift ratio of 2.25%. At the end of the loading, the drift reached 4.0% and severe concrete crushing occurred at the bottom of the columns. It was shown that the proposed frame-wall joints could inhibit out-of-plane movement of the infill wall. The CFS-CLPM composite walls remained quite intact with few spalling of CLPM at failure and the overall damage of CFS-CLPM composite walls in this study was less severe, compared with masonry infill walls in RC frames [23].

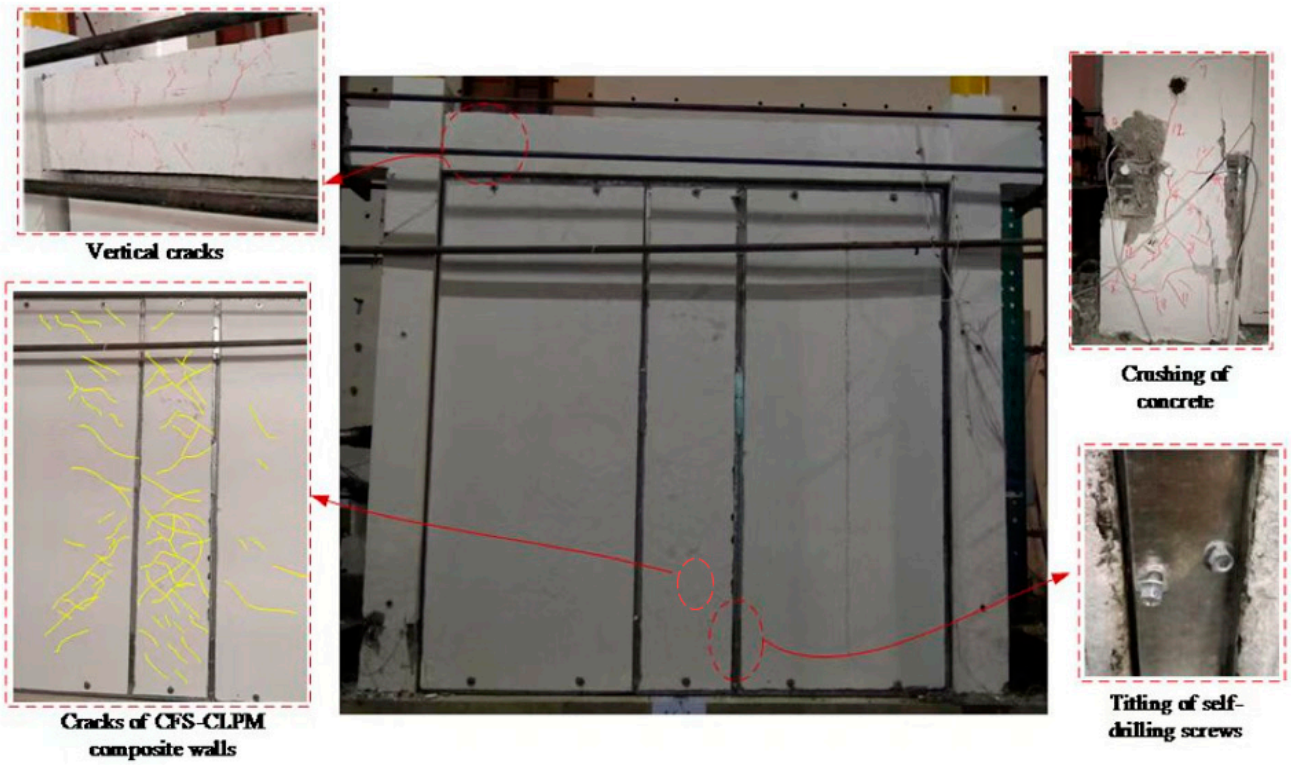

Figure 10. Failure modes of specimen PCFW.

3.2. Hysteretic Response

The load(P)-displacement(Δ) hysteresis curves are plotted in Figure 11. In the initial loading phase, hysteresis curves of all specimens were approximately linear due to the elastic deformation. With the increase of the horizontal displacement, the hysteresis loops exhibited shuttle-shaped when the test specimens reached the elastic–plastic stage. Beyond the peak point, the hysteresis loops of the specimen PCFW transformed to reverse S-shaped owing to the shear deformation including the shear cracks on CFS-CLPM composite walls and the tilting of self-drilling screws along steel trips. In general, the hysteresis loops of PCFW were plumper than that of specimen PCF, which demonstrated that the CFS-CLPM composite infill walls could also dissipate some energy in earthquakes.

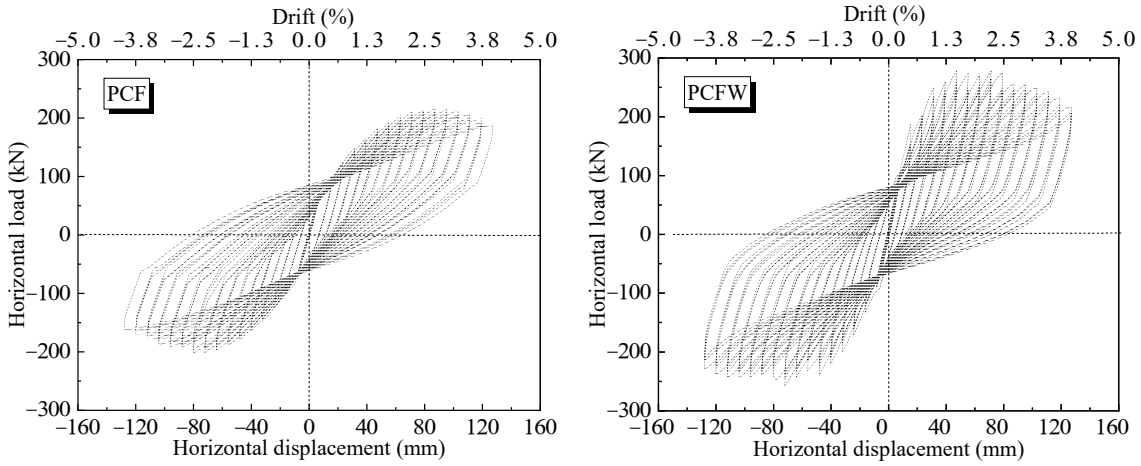

Figure 11. Force–displacement hysteresis curves of specimens.

3.3. Feature Values and Ductility

In this study, envelope curves (Figure 12) were utilized to determine the feature values. The characteristic loads are the yield load P_y, the maximum load P_m, and the failure load P_f, corresponding to the lateral displacement Δ_y, Δ_m, and Δ_f, respectively. The yield point was determined based on the 'graphing method' [24]. The elastic stiffness of the specimens is determined as the secant stiffness at 8 mm displacement in the *P*-Δ curves. Furthermore, the ductility coefficient is defined as $\mu_\Delta = \Delta_f/\Delta_y$. To minimize the errors of μ_Δ, the average μ_Δ was adopted in this study. The feature values of two specimens are listed in Table 3.

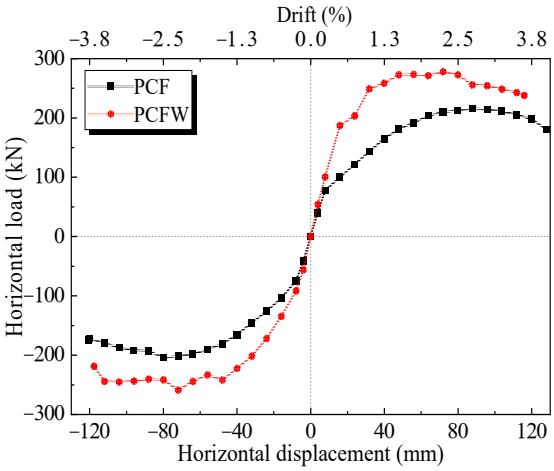

Figure 12. Envelope curves.

Table 3. Feature values of specimens.

Specimen	Δ_y/mm	P_y/kN	Δ_m/mm	P_m/kN	Δ_u/mm	P_f/kN	Elastic Stiffness kN/mm	μ_Δ
PCF (+)	40.9	166.2	88.0	212.58	127.3	180.7	10.22	3.26
PCF (−)	35.4	154.2	80.4	206.62	120.5	175.6	10.50	
PCFW (+)	37.7	248.3	72.0	279.8	116.1	237.8	14.53	3.16
PCFW (−)	36.5	223.2	72.0	258.0	117.7	219.3	14.87	

The effects of the CFS-CLPM composite walls on the cyclic performance of the PC frame were evaluated comprehensively. Specifically, the P_m of specimen PCFW was 24.9~31.6% higher than that of specimen PCF, and the elastic stiffness increased by 34.1~38.4%. The

Δ_y, Δ_m, and Δ_f of PCFW were close to those of PCF and the ductility coefficient of specimen PCFW was 3% lower than that of specimen PCF. However, the failure drifts of PCF and PCFW reached 3.87% and 3.65%, respectively, which can both meet the elastic–plastic drift of 2% required in the Chinese Code for Seismic Design of Buildings [25]. The comparison indicated that CFS-LPM composite walls can improve significantly the load capacity, elastic stiffness of the PC frame, while slightly reducing its ductility because of the infill-frame interaction.

3.4. Energy Dissipation

The energy dissipation capacity of specimens is assessed by calculating the areas of hysteretic loops. Figure 13 illustrates the energy consumption of the 1st loading cycle at each displacement level and cumulative energy dissipation, respectively. It was seen from Figure 13a that the energy consumption of each specimen was less before the displacement level up to 8 mm (drift of 0.25%) owing to the recoverable elastic deformation. Thereafter, it gradually increased as loading displacement increased. Comparisons of the 1st cycle energy consumption between specimens PCF and PCFW demonstrated that additional energy was dissipated by the CFS-CLPM composite walls even at high displacement levels. Furthermore, the cumulative energy of specimen PCFW was 1.14 times higher than that of specimen PCF at the horizontal displacement of 120 mm (drift of 3.75%). The PC frame structure infilled with CFS-CLPM composite walls exhibited better energy dissipation capacity.

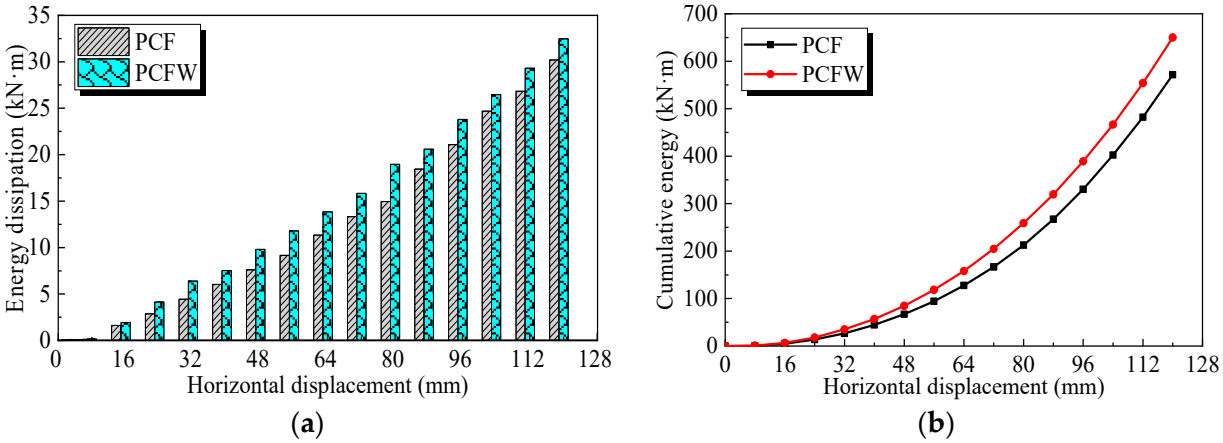

Figure 13. Energy dissipation: (**a**) 1-st cycle energy consumption at each displacement level; (**b**) Cumulative dissipated energy.

3.5. Strain Analyses

Key strains of reinforcement (S1–S6 in Figure 7) were plotted to analyze the influence of the CFS-CLPM composite walls on the strain development of the PC frame. Positive and negative values of the longitude strain represented tension and compression stress, respectively. The yield strain of longitude reinforcements is 2338με according to the material properties results in Section 2.3. As shown in Figure 14, the longitude reinforcements in both specimens yielded by tension earlier than by compression. Owing to the development of typical diagonal strut mechanisms in the infill wall, the higher horizontal load increased the strain of reinforcements around the upper beam–column joint. The strain of reinforcements at column bases was lower since part of the horizontal load was transferred to the infill wall through the compression between columns and infill walls.

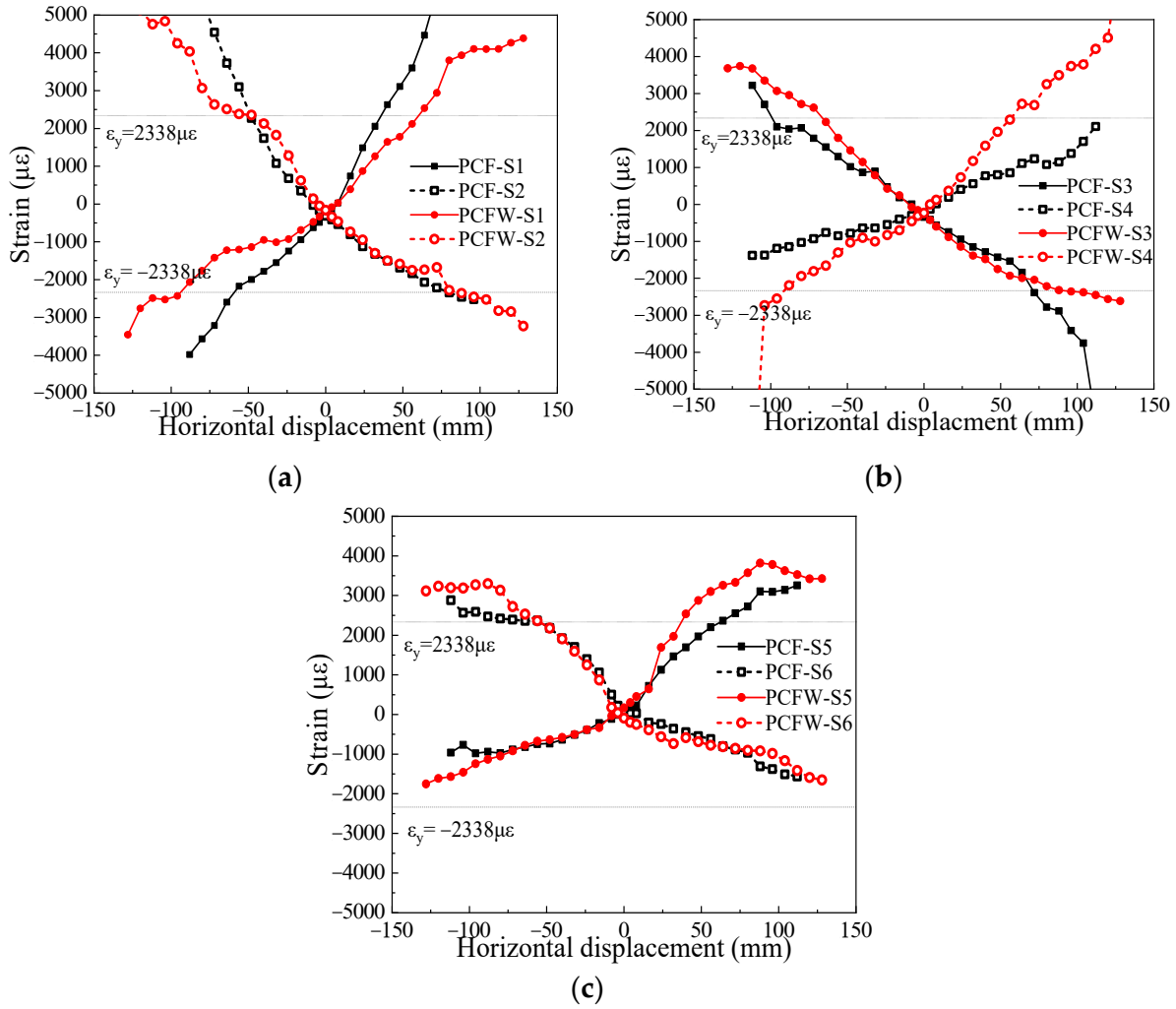

Figure 14. Strain of reinforcements: (**a**) Column feet; (**b**) Column upper ends; (**c**) Beam ends.

4. Numerical Analyses

The specimens examined in Section 2 were modeled by ABAQUS to analyze their lateral performance further in this section. Based on the validated FE models, parametric analyses were conducted to study the influence of dominant parameters, including material, geometric and load cases, on the lateral performance of PC frame structure infilled with CFS-CLPM composite walls.

4.1. Model Characteristics

4.1.1. Material Laws

In the FE modeling, the concrete damaged plasticity (CDP) model was applied to evaluate plastic behaviors of the precast and cast-in-site concrete. The stress–strain behavior of the CDP model was specified following the literature [26]. The bilinear kinematic hardening model (shown in Figure 15) was adopted to describe the stress–strain behavior of steel units of specimens. The f_y and E_s are respectively the yield strength and elastic modulus of the steel, which could be obtained from the preceding coupon tests.

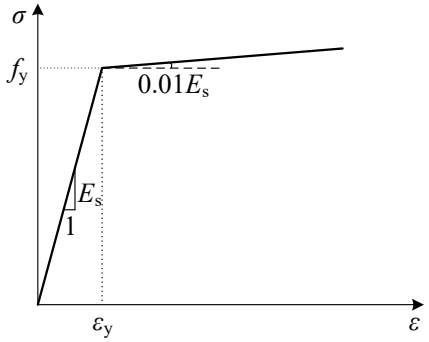

Figure 15. Steel constitutive model.

The CLPM material is essentially similar to the expanded polystyrene (EPS) concrete. Since the constitutive model of CLPM remains obscure at present, the stress–strain model for EPS concrete [27] was employed to simulate the compressive behavior of CLPM, as shown in Equation (1). The tensile strength of CLPM equals to 10% of the maximum compressive strength in this paper.

$$\sigma = \begin{cases} \frac{a(\varepsilon/\varepsilon_{c,m})+(b-1)(\varepsilon/\varepsilon_{c,m})^2}{1+(a-2)(\varepsilon/\varepsilon_{c,m})+b(\varepsilon/\varepsilon_{c,m})^2}\sigma_{c,m} & (0 \le \varepsilon \le \varepsilon_{c,m}) \\ \frac{1+c}{(\varepsilon/\varepsilon_{c,m})^d+c}\sigma_{c,m} & (\varepsilon_{c,m} < \varepsilon \le \varepsilon_{c,u}) \end{cases} \quad (1)$$

in which the parameters a, b, c and d vary with the dry density of CLPM; $\sigma_{c,m}$ is the maximum compressive strength; $\varepsilon_{c,m}$ is the strain corresponding to $\sigma_{c,m}$; $\varepsilon_{c,m}$ is the ultimate compressive strain.

4.1.2. Element Types and Cell Meshing

C3D8R solid elements were applied to concrete and CLPM fillers. Reinforcements were modeled with the T3D2 truss elements. The sleeves and C-section steel were modeled with S4R shell elements. Owing to the few deformations of the foundation during tests, the foundation was considered to be a discrete rigid body. After many attempts, the mesh size of 50 mm was applied for concrete, reinforcements, C-section steel as well as CLPM fillers.

4.1.3. Interaction and Boundary Conditions

In this FE modeling, the reinforcements were rigidly embedded within the concrete neglecting the bond-slip effects at the rebar-concrete interface. The contact surfaces between the precast and cast-in-site concrete were simulated with tie constraints. Based on the experimental phenomena, self-drilling screws used to assemble CFS frames rarely failed and could guarantee reliable connections between wall studs and tracks. Thus, the wall studs and tracks were merged into a whole instance in the FE models. For the CFS-CLPM composite walls, the CFS frame was embedded in the CLPM fillers to improve the convergence of FE models. In addition, the interaction between the beam and steel angles, as well as the foundation and steel angles were defined as tie constraints. Full adherence properties between hook bolts and CFS-CLPM composite walls were assumed by embedding the bolts into CLPM fillers. The behavior of frame-wall joints was simulated by linear springs that were used to describe the welding connections between the hook bolts and the steel angles. The hard contact and penalty with a friction coefficient of 0.3 were adopted to simulate the normal and tangential behavior in the contact surface between the columns and CFS-CLPM composite walls.

In terms of the boundary conditions of the FE models, all translations and rotations of the foundation were restricted to provide fixed properties. Out-of-plane deformation of the FE models was prevented by restricting the displacement and rotational freedoms (U_z, r_{xz}, r_{yz}) of all nodes on the side surfaces of the beam. According to the experimental testing program, axial loads were exerted at the top of each column, and a lateral load was

supplied by the monotonic drifts to simplify the FE models and increase their convergence. Figure 16 shows the FE model details of specimen PCFW as an example.

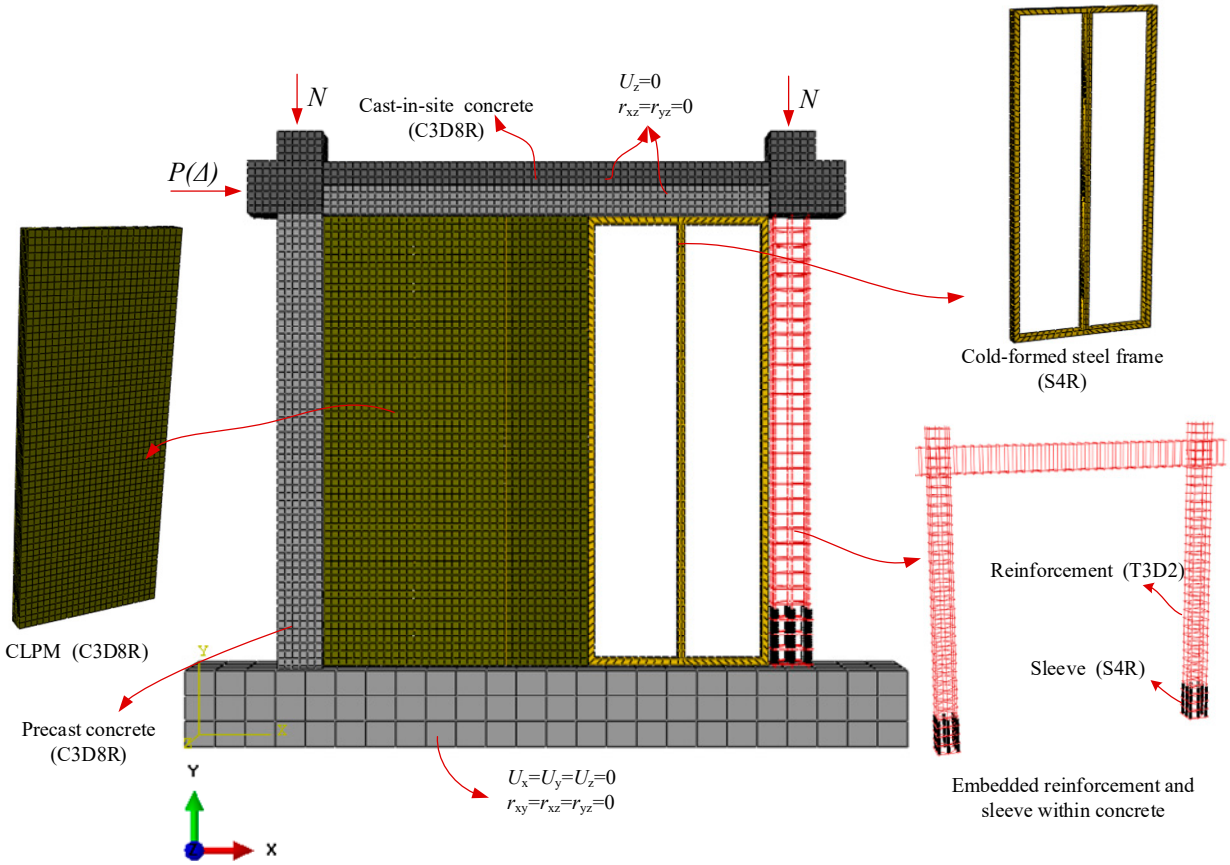

Figure 16. FE model of specimen PCFW.

4.2. Model Validation and Analyses

4.2.1. Model Validation

To verify the accuracy of the FE models, experimental and numerical results of specimens were compared comprehensively, displayed in Table 4 and Figures 17 and 18. The comparison results demonstrated that the FE modeling technique was reasonable to simulate the lateral performance of the PC frame structure.

Table 4. Comparison of experimental and numerical results.

Specimen	Test		Simulation		$K_{e,s}/K_{e,t}$	$P_{m,s}/P_{m,t}$
	$K_{e,t}$ (kN/mm)	$P_{m,t}$ (kN)	$K_{e,s}$ (kN/mm)	$P_{m,s}$ (kN)		
PCF (+)	10.22	212.58	8.53	193.70	0.83	0.91
PCFW (+)	14.53	279.80	15.34	293.31	1.06	1.05

Note: $K_{e,t}$ and $K_{e,s}$ are the elastic stiffness of tested and simulated results, respectively; $P_{m,t}$ and $P_{m,s}$ are the maximum load of tested and simulated results, respectively.

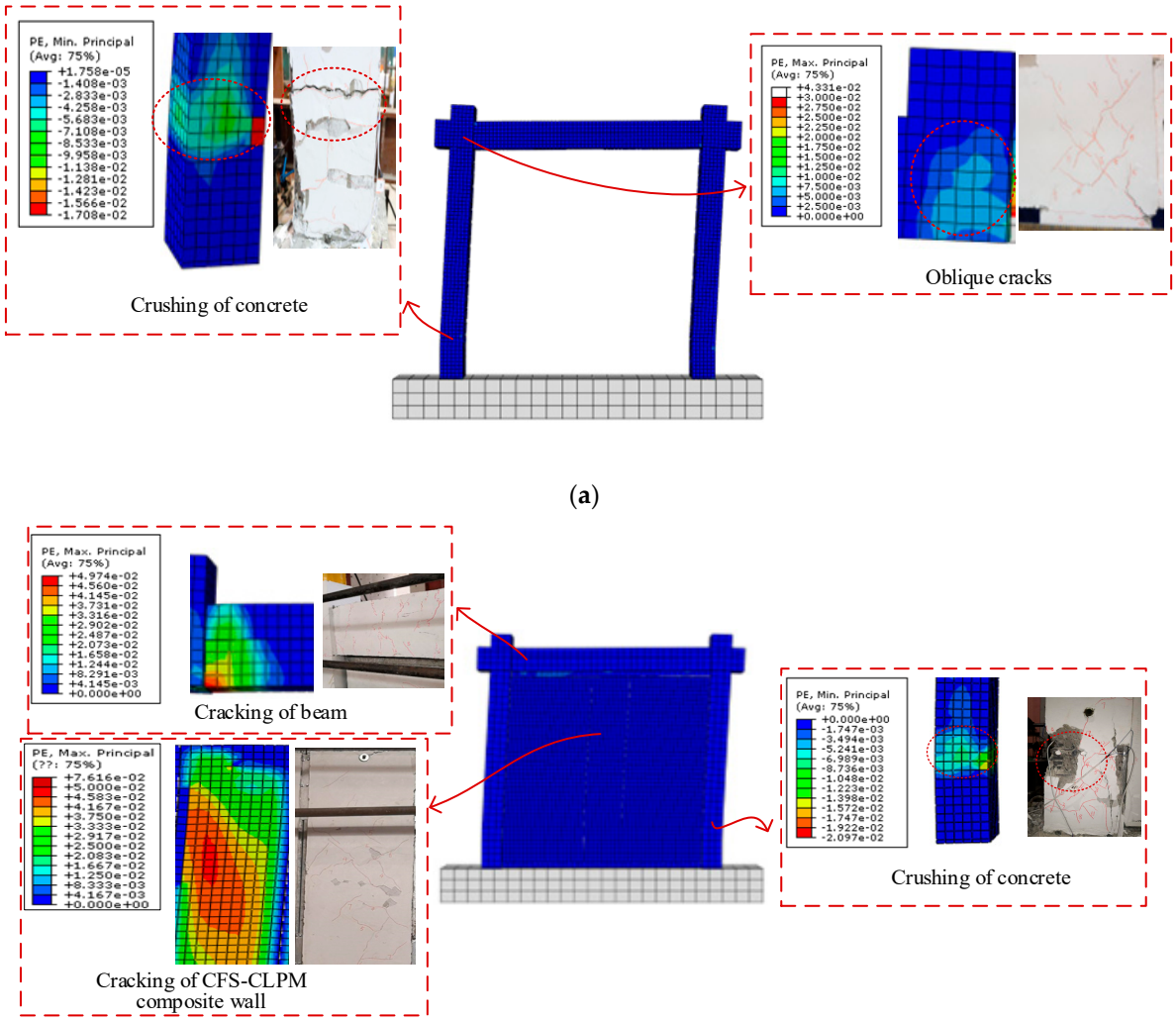

Figure 17. Comparison of failure characteristics: (**a**) PCF; (**b**) PCFW.

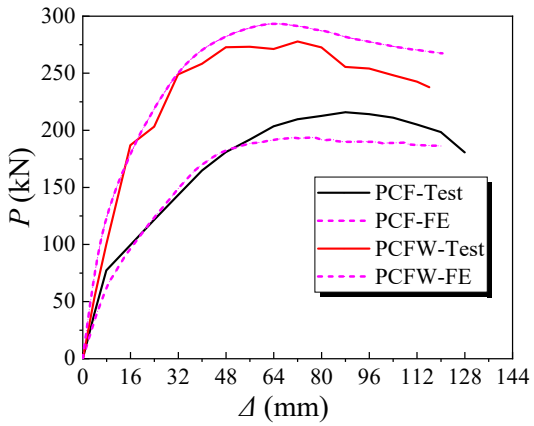

Figure 18. Comparison between experimental and numerical curves.

4.2.2. Contact Stress Distribution

Under horizontal loads, the CFS-CLPM composite walls would be compressed by the PC frame due to the column-wall interaction and wall-frame connections. Figure 19 shows the contact stress distributions on columns for specimen PCFW at various inter-story drifts. It can be seen that the initial contact stress of the left column was primarily distributed

at the top of the column, and then the distribution gradually moved downward along the column. In contrast, the initial contact pressure of the right column occurred mainly at the bottom of the column, followed by two ends and middle regions of the column appeared. These differences in the contact stress distributions are due to the deformation compatibility between the shear deformation of the CFS-CLPM composite walls and the flexural deformation of the PC frame. As the inter-story drifts increased, the contact stress was larger owing to the intensely interactive compression between the columns and CFS-CLPM composite walls.

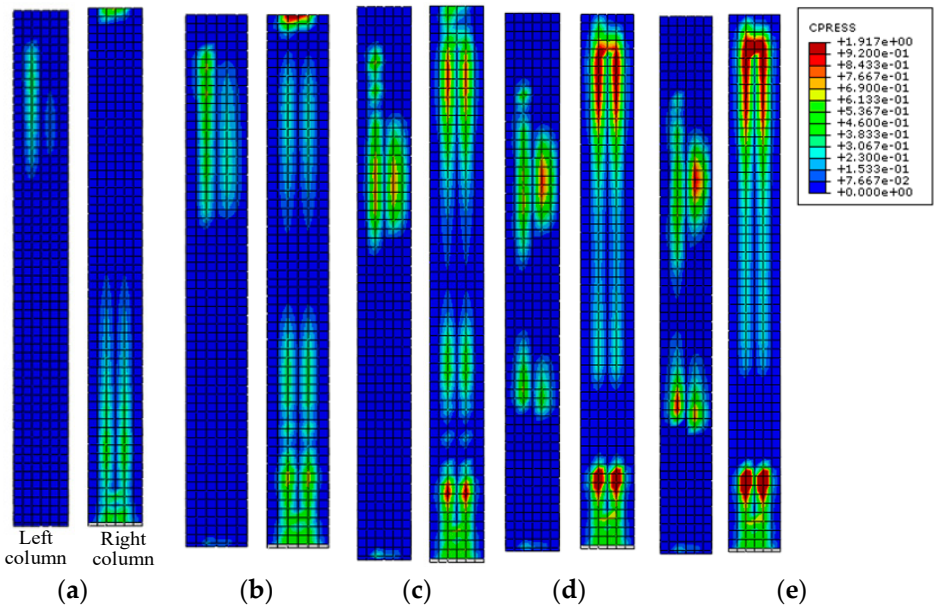

Figure 19. Contact stress distribution on columns for specimen PCFW: (**a**) drift of 0.5%; (**b**) drift of 1.0%; (**c**) peak drift of 2.0%; (**d**) drift of 3.0%; (**e**) drift of 3.65%.

4.2.3. Analyses of the CFS-CLPM Composite Walls

The minimum principal compressive stresses of CLPM are depicted in Figure 20. The compressive stress in Figure 20 was limited to a minimum of −0.92 MPa so that the stress distribution of CLPM was visible. Combined with the contact stress distribution (Figure 19), the compressive zones of the CLPM provided resistance to horizontal loads were marked out in Figure 20a–e with red dashed lines.

It seems that most of the CLPM was compressed at the drift of 0.5%, and the compressive stress was transferred through the diagonal zone of the CLPM. As the inter-story drift increased, horizontal loads transferred to the CFS-CLPM composite walls through the frame-wall joints increased significantly. Consequently, a compressive zone at the top corner of the CLPM was developed at the drift ratio of 1.0%. Compared to the CLPM stress distribution at drift of 0.5%, the diagonal compressive zone of CLPM in Figure 20b enlarged. At the peak drift of 2.0%, there were three compressive zones of CLPM, which were a big compressive zone in the diagonal direction and two small compressive zones near the frame-wall joints. In Figure 20c–e, corresponding to the drift ratio of 2.0–3.65%, the compressive zones of CLPM in the diagonal direction gradually shrunk due to the damage, while two compressive zones of CLPM near the frame-wall joints gradually extended. Eventually, the diagonal compression zone and the compression zone near the lower frame-wall joints merged. The development of the compressive zones indicated that the CFS-CLPM composite walls are considerably involved in resisting the horizontal loads and were damaged eventually. Figure 20f shows contour plots of von Mises stress in the CFS frame at the drift of 3.65%. It was found that the stress of the tracks and studs did not reach its yield strength except in small regions near frame–wall joints.

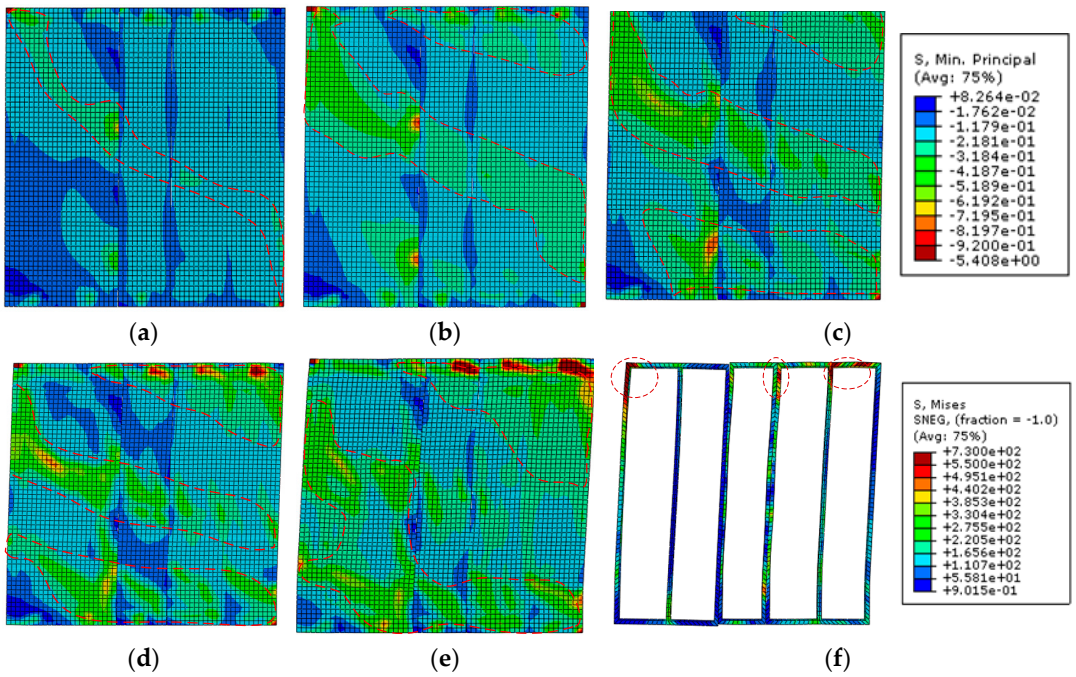

Figure 20. Stress distributions of CFS-CLPM composite walls: (**a**) drift of 0.5%; (**b**) drift of 1.0%; (**c**) peak drift of 2.0%; (**d**) drift of 3.0%; (**e**) drift of 3.65%; (**f**) drift of 3.65%.

4.3. Parametric Analyses

The experimental and numerical analyses above showed that the load capacity and elastic stiffness of the infilled PC frame was improved significantly by the CFS-CLPM composite walls. To explore the influential factors on the lateral response of the PC frame infilled with CFS-CLPM composite walls, parametric analyses using ABAQUS were conducted on material, geometry, and load ratio. The configurations of specimen PCFW were taken as a reference for the simulation sample (FE-SS). The detailed parameters of FE models are listed in Table 5. In order to analyze the influence of the various parameters, the lateral response of this structure was evaluated in terms of the maximum lateral load P_m and elastic stiffness K_e.

Table 5. Parameters of PC frame with CFS-CLPM composite walls.

FE-Models	Material			Geometry		Load Ratio
	f_c/MPa	f_p/MPa	f_y/MPa	L/H	t_w/mm	n
FE-SS	26.8	0.92	550	1.1	130	0.3
FE-11	20.1	0.92	550	1.1	130	0.3
FE-12	33.5	0.92	550	1.1	130	0.3
FE-13	40.2	0.92	550	1.1	130	0.3
FE-21	26.8	1.42	550	1.1	130	0.3
FE-22	26.8	1.92	550	1.1	130	0.3
FE-23	26.8	2.42	550	1.1	130	0.3
FE-31	26.8	0.92	235	1.1	130	0.3
FE-32	26.8	0.92	390	1.1	130	0.3
FE-41	26.8	0.92	550	0.9	130	0.3
FE-42	26.8	0.92	550	1.3	130	0.3
FE-43	26.8	0.92	550	1.7	130	0.3
FE-51	26.8	0.92	550	1.1	160	0.3
FE-52	26.8	0.92	550	1.1	190	0.3
FE-53	26.8	0.92	550	1.1	220	0.3
FE-61	26.8	0.92	550	1.1	130	0.5
FE-62	26.8	0.92	550	1.1	130	0.7
FE-63	26.8	0.92	550	1.1	130	0.85

4.3.1. Compressive Strength of Concrete (f_c)

Figure 21a shows the effect of f_c on the load-displacement curves of the PC frame infilled with CFS-CLPM composite walls. It was seen that, when f_c increased from 20.1 MPa to 26.8 MPa, 33.5 MPa and 40.2 MPa, the P_m increased by 3.11%, 3.36% and 3.42%, respectively, and the K_e increased by 3.35%, 5.7% and 7.30%. This improvement of the P_m and K_e are attributed to the increase of lateral load capacity and initial stiffness of the PC'frame.

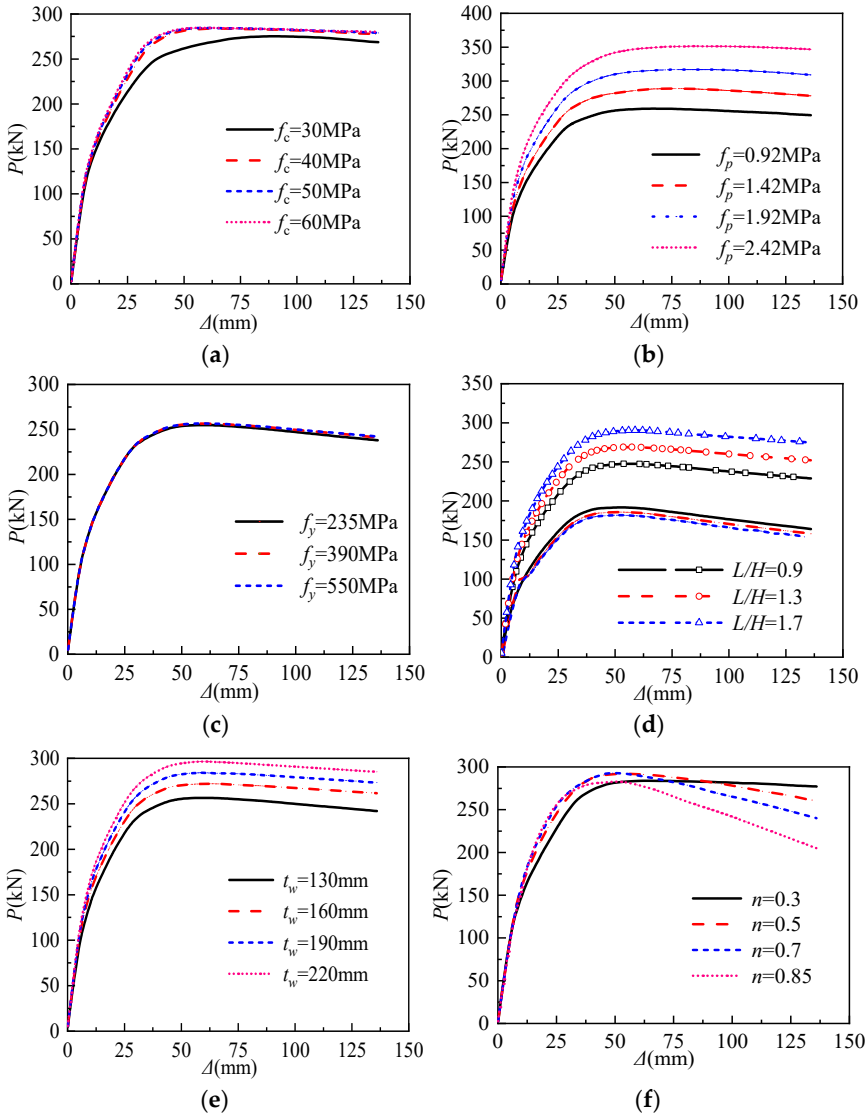

Figure 21. Influence of different parameters on lateral response of PC frame infilled with CFS-CLPM composite walls: (**a**) Compressive strength of concrete; (**b**) Compressive strength of CLPM; (**c**) Strength of cold-formed steel; (**d**) Span to height ratio; (**e**) Thickness of CFS composite walls; (**f**) Axial load ratio.

4.3.2. Compressive Strength of CLPM (f_p)

Figure 21b shows the load–displacement curves of FE models with different compressive strengths of CLPM. As the f_p increased from 0.92 MPa to 1.42 MPa, 1.92 MPa and 2.42 MPa, the P_m improved by 11.44%, 22.26% and 35.56%, respectively. Meanwhile, the K_e improved by 10.21%, 21.44% and 33.31%, respectively. It could be found that both P_m and K_e are almost improved linearly with the increase of the f_p. This phenomenon confirmed further that the parameter of f_p has a significant influence on the lateral response of the PC frame infilled with CFS-CLPM composite walls, and the CLPM fillers are important lateral resistance elements of the CFS-CLPM composite walls.

4.3.3. Strength of Cold-Formed Steel (f_y)

In the numerical analyses of the CFS-CLPM composite walls, Figure 20f shows that most of the CFS frame does not reach its yield strength. Therefore, a lower f_y was selected in parametric analyses. Figure 21c illustrates the numerical results of the structure with f_y of 235 MPa, 390 MPa, and 550 MPa. The load-displacement curves of the structure with f_y of 235 MPa and 345 MPa almost coincided with that of the structure with f_y of 550 MPa. This demonstrates that f_y has little effect on the lateral performance of the structure and it is suggested to reduce the strength of the cold-formed steel appropriately to lower the overall cost of the CFS-CLPM composite walls in engineering projects.

4.3.4. Span to Height Ratio (L/H)

The span and height of the structure were defined as depicted in Figure 3a. The FE models with different ratios (L/H) were featured with a constant height (H = 3030 mm), while the span (L) was taken as 2700 mm, 3900 mm and 5100 mm, corresponding to L/H of 0.9, 1.3 and 1.7, respectively. As L increased from 2700 to 5100 mm, the number of the separated CFS-CLPM composite walls with width of 1200 mm rose from 2 to 4.

To highlight the mechanical contribution of CFS-CLPM composite walls to the PC frame structures, the parametric analyses of L/H were conducted not only on the infilled PC frames with CFS-CLPM composite walls but also on the corresponding bare PC frames. Figure 21d shows the load-displacement curves, in which the curves of the infilled PC frame were lines with symbols. Under L/H of 0.9, P_m and K_e of the infilled PC frame were respectively 29.13% and 18.06% higher than that of the bare PC frame. Similarly, setting the bare PC frames as a benchmark at the same ratio of L/H, P_m and K_e of the infilled PC frame with L/H of 1.3 were increased by 44.83% and 26.85%, respectively, and those of the infilled PC frame with L/H of 1.7 were increased by 59.58% and 50%, respectively. It is seen that the CFS-CLPM composite walls have a notable improvement on the P_m of the PC frame structure, especially on K_e. Hence, it is suggested that the lateral load capacity and stiffness provided by the CFS-CLPM composite infill walls should be included in the lateral resistance of the infilled PC frame structure.

On the other hand, it was noted that the P-Δ curves of the bare PC frames with different L/H were almost same. On this basis, it was assumed herein that the lateral resistance contributed by the PC frame of the infilled PC frame structure was nearly identical under different L/H. Thus, compared to the P_m and K_e of the infilled PC frame structure with L/H of 0.9, P_m of the structure with L/H of 1.3 and 1.7 respectively increased by 7.99% and 16.70%, and K_e respectively increased by 7.54% and 16.63%. Generally, the span-to-height ratio of the CFS-CLPM composite walls can significantly influence the lateral response of PC frame structures.

4.3.5. Thickness of CFS-CLPM Composite Walls (t_w)

Various t_w of 130 mm, 160 mm, 190 mm and 220 mm were investigated, as depicted in Figure 21e. Compared with the numerical results with t_w of 130 mm, P_m of the structure with t_w of 160 mm, 190 mm and 220 mm increased by 6.04%, 10.74% and 15.57%, respectively. Meanwhile, K_e of the structure with t_w of 160 mm, 190 mm and 220 mm were 8.61%, 13.11% and 17.72% higher, respectively. Although the P_m and K_e of the infilled PC frame structures are enhanced to some extent by increasing of t_w, there are some disadvantages such as more expensive cost, heavier weight for the walls, and less available space of the buildings. Therefore, the thickness of the CFS-CLPM composite walls should be selected after comprehensive consideration.

4.3.6. Axial Load Ratio (n)

In view of the variation of axial loads imposed on columns in engineering practices, n varied from 0.3 to 0.85 were considered, as shown in Figure 21f. Compared to the numerical results with n of 0.3, P_m of the structure with n of 0.5, 0.7 and 0.85 were 3.87%, 4.23% and 0.66% higher, respectively, and K_e of the structure with n of 0.5, 0.7 and 0.85 were

1.01%, 0.16% higher and 3.64% lower, respectively. It can be concluded that axial loads have a minor effect on the P_m and K_e of the infilled PC frame structures, but they have a measurably adverse influence on the ductility of the structure due to the premature failure of concrete and the intensification of the second-order effects.

5. Prediction of the Elastic Stiffness

Elastic stiffness is decisive indexes for the serviceability limit state of structures and a number of researches have been conducted on the prediction method of elastic stiffness of members and structures [28]. Based on the experimental and parametric results, the elastic lateral stiffness of the infilled PC frame structure can be greatly enhanced by the CFS-CLPM composite walls. However, the lateral stiffness of the infill walls was always ignored in the previous design model of the PC frame structure, which would not effectively utilize the structural performance of the PC frame infilled with CFS-CLPM composite walls. Hence, the contribution of the CFS-CLPM composite walls was considered to accurately estimate the elastic stiffness of the infilled PC frame structure under horizontal loads in this study. The elastic lateral stiffness K of the infilled PC frame structure is provided by the PC frame and CFS-CLPM composite walls, and defined as Equation (2):

$$K = K_f + K_W \tag{2}$$

where K_f is the elastic lateral stiffness of the PC frame, and K_w is the elastic lateral stiffness of the CFS-CLPM composite walls.

Under horizontal loads, the Muto's method (modified D-method) was adopted to calculate the K_f provided by two columns of the PC frame [29]. Thereby, K_f can be obtained by Equation (3), and the relevant variables are expressed in Equations (4)–(6):

$$K_f = 2(\zeta \frac{12 i_c}{{h_c}^2}) \tag{3}$$

$$i_m = \frac{E_m I_m}{l_m} \tag{4}$$

$$\zeta = \begin{cases} \frac{k}{2+k}, \text{ columns of typical floor} \\ \frac{0.5+k}{2+k}, \text{ columns of ground floor} \end{cases} \tag{5}$$

$$k = \begin{cases} \frac{i_1+i_2+i_3+i_4}{2i_c}, \text{ columns of typical floor} \\ \frac{i_1+i_2}{i_c}, \text{ columns of ground floor} \end{cases} \tag{6}$$

where E_m is the elastic modulus of members; I_m is the inertia moment of member sections; l_m is the length of members; i_m is the line stiffness for members; h_c is the height of columns; i_c is the line stiffness for columns, and i_1~i_4 are the line stiffness of beams surrounding the column as shown in Figure 22.

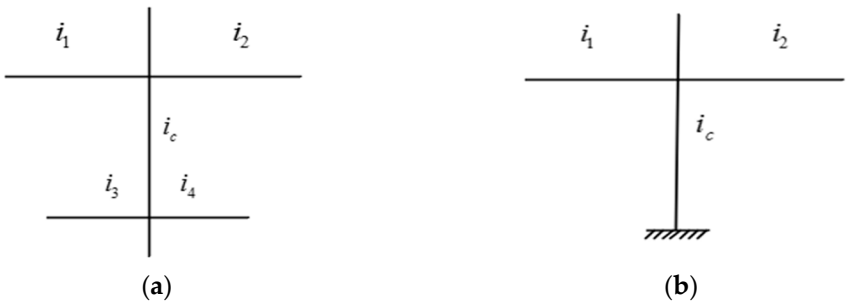

Figure 22. Line stiffness of components for a typical floor or ground floor: (**a**) typical floor; (**b**) ground floor.

Under horizontal loads, the horizontal displacements of the CFS-CLPM composite walls are induced by the shear and flexural deformation derived from a combination of the CFS frame and the CLPM fillers. In the assembly of the CFS frame, the studs were connected to the tracks using self-drilling screws that were assumed to be hinge joints in mechanical behavior. On the basis of the above assumptions, the horizontal displacement of the CFS-CLPM composite walls was determined by the shear and flexural deformation of the CLPM fillers, and was expressed as follows [11]:

$$\Delta = \frac{1.2PH}{GtL} + \frac{PH^3}{3EI} \tag{7}$$

where P is the horizontal load carried by CFS-CLPM composite walls; H, L, and t are the height, width, and thickness of the CLPM fillers, respectively; G and E are the shear and elastic modulus of the CLPM, respectively. I is the inertia moment of the CLPM fillers section. Thereby, the calculation formula of K_w is described as Equation (8):

$$K_w = \frac{P}{\Delta} = \frac{1}{\frac{1.2H}{GtL} + \frac{H^3}{3EI}} \tag{8}$$

Therefore, the elastic stiffness of the infilled PC frame structure can be calculated by substituting Equations (3) and (8) into Equation (2). The deduced formula is expressed as follows:

$$K = 2(\zeta \frac{12i_c}{h^2}) + \frac{1}{\frac{1.2H}{GtL} + \frac{H^3}{3EI}} \tag{9}$$

To verify the reliability, Equation (9) was adopted to predict the initial stiffness of specimens in Sections 3 and 4. The predictions were compared to the simulations and test results as listed in Table 6. The average ratio of K_p/K_t is 1.005 with a variation of 0.0021, which indicates that the proposed calculation method can work well for predicting the elastic lateral stiffness of the PC frame infilled with CFS-CLPM composite walls.

Table 6. Comparison of predicted lateral stiffness results.

Samples	K_t (kN/mm)	K_p (kN/mm)	K_p /K_t
PCF	10.22	10.347	1.012
PCFW	14.53	14.878	1.023
PE-SS	14.967	14.907	0.996
FE-21	16.604	16.375	0.986
FE-22	18.358	17.836	0.972
FE-23	20.14	19.297	0.958
FE-41	14.21	13.192	0.921
FE-42	15.67	15.73	1.004
FE-43	17.54	19.482	1.111
FE-51	15.867	15.967	1.006
FE-52	16.565	17.021	1.028
FE-53	17.269	18.075	1.047
Average	-	-	1.005
Coefficient of variation	-	-	0.0021

Note: K_t is the tested or simulated elastic lateral stiffness; K_p is the predicted elastic lateral stiffness.

6. Conclusions

In this paper, the prefabricated CFS-CLPM composite walls were adopted into the PC frame. The cyclic tests were performed to investigate the influence of the CFS-CLPM composite walls on the seismic response of the PC frame structure. Numerical simulations and analytical prediction of elastic stiffness were conducted further on the PC frame

infilled with CFS-CLPM composite walls to systematically study the lateral behavior. The conclusions can be summarized as follows:

1. The failure modes of the PC frame infilled with CFS-CLPM composite walls were characterized by cracks on the PC frame, diagonal cracks on the CFS-CLPM composite walls, titling of self-drilling screws, and crushing of the columns. The CFS-CLPM composite walls remained quite intact and the proposed wall-frame joints could restrain out-of-plane movements of the walls even at failure.
2. The CFS-CLPM composite walls can significantly improve the lateral behavior of the PC frame structure. Compared with the bare frame, the lateral load capacity and elastic stiffness of the infilled frame were respectively 24.9~31.6% and 34.1~38.4% higher, respectively. Moreover, the energy dissipation capacity of the infilled frame structure increased by 14%. Despite a slight reduction in the ductility of the infilled PC frame structure owing to the infill-frame interaction, its failure drift can meet the elastic-plastic drift requirement of 2%.
3. The numerical analyses of the infilled PC frame structure revealed that CLPM fillers were the significant lateral resistance elements of the CFS-CLPM composite walls. Three compressive zones were formed on the CLPM fillers, because the horizontal shear force was transferred from the PC frame to CFS-CLPM composite walls through the frame-wall joints between the composite wall and PC beam, and the compression between the composite wall and the PC column.
4. Parametric analyses of the PC frame infill with CFS-CLPM composite walls indicated that the strength of CLPM, the span-to-height ratio, and the thickness of CFS-CLPM composite walls significantly affected the lateral capacity of the structure, while the strength of concrete, the strength of cold-formed steel and the axial load ratio affected slightly.
5. A formula considering the lateral resistance of the CFS-CLPM composite walls was proposed to predict the elastic lateral stiffness of the PC frame infilled with CFS-CLPM composite walls and the comparisons among prediction and test as well as simulation results demonstrated that the formula was reliable.

Author Contributions: Software, data curation, visualization, writing—original draft preparation, P.H.; writing—review and editing, methodology, formal analysis, Y.L.; funding acquisition, supervision, resource, J.W.; conceptualization, validation, W.W.; formal analysis, investigation, data curation G.P. All authors have read and agreed to the published version of the manuscript.

Funding: This research was funded by the Special Funds for the Central Universities of China (No. PA2021KCPYO031), the Fundamental Research Funds for the Central Universities of China (No. PA2021GDSK0078, JZ2021HGTA0158), the Natural Science Research Project of China (No. 52278170), and the Natural Science Research Project of Anhui Province (No. 2108085QE248).

Institutional Review Board Statement: Not applicable.

Informed Consent Statement: Not applicable.

Data Availability Statement: Not applicable.

Conflicts of Interest: The authors declare no conflict of interest.

References

1. Badr, A.R.; Elanwar, H.H.; Mourad, S.A. Numerical and experimental investigation on cold-formed walls sheathed by fiber cement board. *J. Constr. Steel Res.* **2019**, *158*, 366–380. [CrossRef]
2. Macillo, V.; Fiorino, L.; Landolfo, R. Seismic response of CFS shear walls sheathed with nailed gypsum panels: Experimental tests. *Thin-Walled Struct.* **2017**, *120*, 161–171. [CrossRef]
3. Ali, E.; Althoey, F. Numerical investigation on blast response of cold-formed steel framing protected with functionally graded composite material. *Buildings* **2022**, *12*, 118. [CrossRef]
4. Xu, Z.F.; Chen, Z.F.; Osman, B.H.; Yang, S.H. Seismic performance of high-strength lightweight foamed concrete-filled cold-formed steel shear walls. *J. Constr. Steel Res.* **2018**, *143*, 148–161. [CrossRef]

5. Ananthi, G.B.G.; Roy, K.; Lim, J.B.P. Experimental and numerical study of an innovative 4-channels cold-formed steel built-up column under axial compression. *Steel Compos. Struct.* **2022**, *42*, 513–538.
6. Ananthi, G.B.G. A study on cold-formed steel compound angle section subjected to axial compression. *KSCE J. Civ. Eng.* **2018**, *22*, 1803–1815. [CrossRef]
7. Mousavi, S.A.; Zahrai, S.M.; Bahrami-Rad, A. Quasi-static cyclic tests on super-lightweight EPS concrete shear walls. *Eng. Struct.* **2014**, *65*, 62–75. [CrossRef]
8. Shannag, M.J. Characteristics of lightweight concrete containing mineral admixtures. *Constr. Build. Mater.* **2011**, *25*, 658–662. [CrossRef]
9. Mydin, M.A.O.; Wang, Y.C. Structural performance of lightweight steel-foamed concrete-steel composite walling system under compression. *Thin-Walled Struct.* **2011**, *49*, 66–76. [CrossRef]
10. Yin, C.; Zhou, L.; Zou, Q.Y.; Xu, Y.F. Effect of filling phosphorgypsum on the axial compression behavior of cold-formed thin-walled steel walls. *Buildings* **2022**, *12*, 1325. [CrossRef]
11. Wu, H.H.; Sui, L.; Wang, J.Q.; Zhou, T.H. Cycle performance tests and numerical modeling of infilled CFS shear wall. *J. Constr. Steel Res.* **2020**, *168*, 106010. [CrossRef]
12. Wang, W.Q.; Wang, J.F.; Zhao, P.; Ja, L.L.; Pan, G.D. Axial compressive experiments and structural behaviour estimation of CFS composite walls sprayed with LPM. *J. Build. Eng.* **2020**, *30*, 101305. [CrossRef]
13. Wang, W.Q.; Wang, J.F.; Guo, L.; Liu, Y.; Zhang, R. Cyclic performance tests and numerical analysis of prefabricated CFS shear walls filled with lightweight EPS mortars. *Eng. Struct.* **2021**, *243*, 112554. [CrossRef]
14. Wang, J.Q.; Zhou, T.H.; Wu, H.H.; Guan, Y.; Zhang, L. Cyclic performance of steel frame fabricated with cold-formed steel composite wall structure. *Eng. Struct.* **2022**, *270*, 114892. [CrossRef]
15. Wang, F.L.; Yang, J.; Wang, X.; Azim, I. Study on progressive collapse behaviour of steel-framed substructures with sheathed CFS stud infill walls. *J. Build. Eng.* **2021**, *42*, 102720. [CrossRef]
16. Kildashti, K.; Samali, B.J.; Mortazavi, M.; Ronagh, H.; Sharafi, P. Seismic collapse assessment of a hybrid cold-formed hot-rolled steel building. *J. Constr. Steel Res.* **2019**, *155*, 504–516. [CrossRef]
17. *JGJ 355-2015*; Technical Specification for Grout Sleeve Splicing of Rebars. China Architecture & Building Press: Beijing, China, 2015.
18. *GB/T 51231-2016*; Technical Standard for Assembled Buildings with Concrete Structure. China Architecture & Building Press: Beijing, China, 2017.
19. 19. *JGJ 1-2014*; Technical Specification for Precast Concrete Structures. China Architecture & Building Press: Beijing, China, 2014.
20. *GB/T 50081-2002*; Standard for Test Method of Mechanical Properties on Ordinary Concrete. China Architecture & Building Press: Beijing, China, 2003.
21. *JG/T 266-2011*; Foamed Concrete. Architecture & Industry Press of China: Beijing, China, 2011.
22. *GB/T 228.1-2010*; Metallic Materials-Tensile Testing-Part 1: Method of Test at Room Temperature. General Administration of Quality Supervision, Inspection of PR China: Beijing, China, 2012.
23. Dautaj, A.D.; Kadiri, Q.; Kabash, N. Experimental study on the contribution of masonry infill in the behavior of RC frame under seismic loading. *Eng. Struct.* **2018**, *165*, 27–37. [CrossRef]
24. Dabiri, H.; Kaviani, A.; Kheyroddin, A. Influence of reinforcement on the performance of non-seismically detailed RC beam-column joints. *J. Build. Eng.* **2020**, *31*, 101333. [CrossRef]
25. *GB 50011-2010*; Code for Seismic Design of Buildings. China Architecture & Building Press: Beijing, China, 2010.
26. Popovics, S. A numerical approach to the complete stress-strain curve of concrete. *Cem. Concr. Res.* **1973**, *3*, 583–599. [CrossRef]
27. Cui, C.C.; Huang, Q.; Li, D.B.; Quan, C.R.; Li, H.C. Stress–strain relationship in axial compression for EPS concrete. *Constr. Build. Mater.* **2016**, *105*, 377–383. [CrossRef]
28. Lai, B.L.; Yang, L.F.; Xiong, M.X. Numerical simulation and data-driven analysis on the flexural performance of steel reinforced concrete composite members. *Eng. Struct.* **2021**, *247*, 113200. [CrossRef]
29. Mutō, K. *Aseismic Design Analysis of Buildings*; Maruzen Company, Ltd.: Tokyo, Japan, 1974.